Journal of MATERIALS RESEARCH

Invited Paper
DOI: 10.1557/jmr.2018.431

INTRINSIC AND EXTRINSIC SIZE EFFECTS IN MATERIALS

FOCUS ISSUE

Size-dependent vibration analysis of carbon nanotubes

Wu-Rong Jian[1], Xiaohu Yao[1,a], Yugang Sun[1], Zhuocheng Xie[1], Xiaoqing Zhang[1]

[1]Department of Engineering Mechanics, South China University of Technology, Guangzhou, Guangdong 510640, People's Republic of China
[a)]Address all correspondence to this author. e-mail: yaoxh@scut.edu.cn

Received: 5 September 2018; accepted: 29 October 2018

Considering the nonlocal small-scale effect and surface effect, we perform the size-dependent vibration analysis of carbon nanotube (CNT). The modified governing equations for CNT's vibration behaviors are derived by using the nonlocal Euler–Bernoulli and Timoshenko beam models, together with the consideration of surface tension and surface elasticity. According to the numerical experiments, both small-scale effect and surface effect make a substantial difference. For flexural vibration, size effect for CNT's vibration behaviors weakens with the increase of its diameter, but strengthens with the increase of the length–diameter ratio; for shear vibration with constant length–diameter ratio, a nonlinear correlation between size effect and CNT's diameter exists, suggesting that there is a typical diameter for CNTs, which corresponds to the "strongest" size effect. In addition, the effects of elastic substrate modulus, temperature change, and axial preloading on the vibration behaviors and their size-dependence are analyzed, respectively.

Introduction

As a unique one-dimension material, carbon nanotube (CNT) has exceptional mechanical and physical properties, including high tensile strength [1, 2], strength-to-weight ratio [3], and Young's modulus [4]. In addition, their excellent thermal, electronic, gas-storage, and fluid-conveying properties [5] are attracting more and more attention and also bear potential applications in the nanoelectromechanical systems, such as nanoresonators [6, 7], nanomotor [8], nanogear [9], and nanoactuator [10]. All of these applications are closely connected with the vibration behaviors of CNTs. To better design novel nanodevices, CNT's vibration analysis is inevitable and plays an important role in the practical application.

Currently, CNT's vibration analysis is mainly carried out by molecular dynamics (MD) simulations [11, 12, 13, 14, 15, 16] and nonlocal continuum mechanical models [17, 18, 19, 20, 21, 22, 23, 24, 25, 26, 27]. Because of the difficulties associated with probing atomic-level structures via laboratory apparatuses in some cases, the former can be a good supplement to the experiments. Using MD simulations, CNT's vibration behaviors can be simulated accurately by calculating the positions of all the carbon atoms, given the utilization of proper potentials, e.g., the interatomic potential developed by Tersoff [28], the reactive empirical bond order potential [29], or the adaptive intermolecular reactive empirical bond order potential [30]. However, fully MD simulations in the engineering cases would be extremely difficult and computationally expensive. Therefore, simplified mechanical models are necessary to predict the vibration behaviors of CNTs and improve the mechanical performance of nanodevices consisting of CNTs.

Different from the macroscopic materials, the mechanical properties of nanomaterials, e.g., CNTs, show remarkable size dependence. As their dimensions decrease continuously at the nanoscale, the surface-to-volume ratio increases rapidly, which influences the mechanical performance of nanomaterials to a large extent. Thus, both small-scale effect and surface effect should be considered. To describe the small-scale effect accurately, nonlocal elasticity theory [31] is proposed to build the nonlocal continuum mechanical models. Based on this theory, the stress at a material point acts as the function of the strains at all points in the body. In this way, the small-scale effect is captured. Recently, researchers have implemented such a theory to investigate the vibration behaviors of CNTs. Various nonlocal beam theories are used to study the vibration responses of single-walled CNTs and multiwalled CNTs with different boundary conditions [17, 18, 19, 20, 21]. Herein, CNTs with different lengths and diameters are discussed. In addition, the effects of elastic substrate modulus [22, 23, 24], temperature change [25], and axial preloading [26, 27], on the

https://doi.org/10.1557/jmr.2018.431 Published online by Cambridge University Press

© Materials Research Society 2019

vibration behaviors are also investigated, based on one or more nonlocal beam models. Nevertheless, the research results from different nonlocal beam models, such as nonlocal Timoshenko and Euler–Bernoulli beam models, have not been compared in detail. Moreover, the surface effect on the vibration response is also untouched.

In this work, we analyze the size effect on the vibration response of CNTs. First, size effects, including the nonlocal small-scale effect and surface effect, are demonstrated by deriving the modified nonlocal Euler–Bernoulli and Timoshenko beam models for vibration analysis. Second, numerical experiments are carried out to obtain the vibration characteristics of CNTs with consideration of different vibration mode order and the fundamental response of the circular frequency to their dimension. Finally, the influences of several factors, i.e., elastic substrate modulus, temperature change, and axial preloading, on the circular frequency and their size-dependence are also illustrated.

Size effect

Small-scale effect and surface effect are two typical characteristics of size effect for nanomaterials. For small-scale effect, nonlocal elastic model, rather than classical continuum model, is implemented to describe accurately the mechanical performance of CNTs, and the corresponding elastic constitutive equation can be shown as [32]

$$\begin{cases} \sigma(x) - (e_0 a)^2 \frac{\partial^2 \sigma(x)}{\partial x^2} = E\varepsilon(x) \\ \tau(x) - (e_0 a)^2 \frac{\partial^2 \tau(x)}{\partial x^2} = G\gamma(x) \end{cases} . \quad (1)$$

Herein, $\sigma(x)$ and $\tau(x)$ are normal and shear stresses on the cross section along the longitudinal direction of CNTs, respectively. $\varepsilon(x)$ and $\gamma(x)$ are the corresponding normal and shear strains. e_0 is a material constant which can be determined through MD simulations, and a is the internal characteristic length. Besides, E and G are the Young's modulus and shear modulus of CNTs, respectively.

For surface effect, surface elasticity and surface stress are taken into account. The effective flexural rigidity $(EI)^*$ of CNTs is given as [32]

$$(EI)^* = EI + \frac{\pi}{8} S(d+t)^3 \quad , \quad (2)$$

where I, S, d, and t are the bending rotary inertia of the cross section, the surface modulus, CNT's diameter, and its wall thickness, respectively. It is worth noting that we focus on the vibration behavior of single-walled CNTs embedded in the elastic substrate. For simplification, only simply supported boundary condition at the two ends is discussed.

Modified Euler–Bernoulli beam model

For Euler–Bernoulli beams, shear deformation and cross-sectional rotary inertia are neglected. Similar to the form for the classical Euler–Bernoulli beam theory, the differential governing equation for CNT's vibration behavior with consideration of small-scale effect and surface effect can be given as

$$\begin{aligned} (EI)^* \frac{\partial^4 w}{\partial x^4} + \left[-(N+H^0) \frac{\partial^2 w}{\partial x^2} + (e_0 a)^2 (N+H^0) \frac{\partial^4 w}{\partial x^4} \right] \\ + \left[\rho A \frac{\partial^2 w}{\partial t^2} - (e_0 a)^2 \rho A \frac{\partial^4 w}{\partial x^2 \partial t^2} \right] = 0 \end{aligned} \quad , \quad (3)$$

where A, w, ρ, and N are the cross-sectional area, the beam deflection, the mass density, and the axial load, respectively. In addition, $H^0 = 2\tau_0(d+t)$, where τ_0, d, and t are CNT's residual surface stress, its diameter, and wall thickness, respectively. Thus, the internal forces can be expressed as

$$\begin{cases} M = -(EI)^* \frac{\partial^2 w}{\partial x^2} - (e_0 a)^2 \left[(N+H^0) \frac{\partial^2 w}{\partial x^2} - \rho A \frac{\partial^2 w}{\partial t^2} \right] \\ Q = -(EI)^* \frac{\partial^3 w}{\partial x^3} - (e_0 a)^2 \left[(N+H^0) \frac{\partial^3 w}{\partial x^3} - \rho A \frac{\partial^3 w}{\partial x \partial t^2} \right] \end{cases} , \quad (4)$$

where M is the bending moment and Q is the shear force on the cross section. Based on the separated variable method, the general solution of Eq. (3) can be given as

$$w(x,t) = W(x) e^{i\omega t} \quad . \quad (5)$$

Substituting Eq. (5) into Eq. (3), one can obtain

$$\begin{cases} \left[(EI)^* + (e_0 a)^2 (N+H^0) \right] \frac{\partial^4 W}{\partial x^4} \\ + \left[(e_0 a)^2 \omega^2 \rho A - (N+H^0) \right] \frac{\partial^2 W}{\partial x^2} - \omega^2 \rho A W = 0 \\ G_1 \frac{\partial^4 W}{\partial x^4} + G_2 \frac{\partial^2 W}{\partial x^2} + G_3 W = 0 \end{cases} . \quad (6)$$

Herein, $G_1 = (EI)^* + (e_0 a)^2 (N + H^0)$, $G_2 = -(N + H^0) + (e_0 a)^2 \omega^2 \rho A$, and $G_3 = -\omega^2 \rho A$. The general solution of Eq. (6) is

$$W(x) = c_1 \sin(\alpha x) + c_2 \cos(\alpha x) + c_3 e^{\beta x} + c_4 e^{-\beta x} \quad , \quad (7)$$

where $\alpha > 0$, $\beta > 0$, $\alpha^2 = \frac{\sqrt{G_2^2 - 4G_1 G_3} + G_2}{2G_1}$, and $\beta^2 = \frac{\sqrt{G_2^2 - 4G_1 G_3} - G_2}{2G_1}$. Then,

https://doi.org/10.1557/jmr.2018.431 Published online by Cambridge University Press

© Materials Research Society 2019

$$\omega^2 = \frac{\left[(EI)^* + (e_0a)^2(N+H^0)\right]\alpha^2 + (N+H^0)}{\left[1+(e_0a)^2\alpha^2\right]\rho A}\alpha^2 \quad , \quad (8)$$

where we can find the size effect by comparing this solution [Eq. (8)] and the classical solution $\left(\omega_{EB}^0 = \alpha^2\sqrt{\frac{EI}{\rho A}}\right)$. In this way, size-dependent vibration analysis of CNTs can be simplified into the determination of α with the simply supported boundary condition at the two ends. Herein, the value of α should avoid the possible situation where c_1, c_2, c_3, and c_4 in Eq. (7) have the value of zero at the same time. Combining Eqs. (4), (5), and (7), we can obtain the rotation angel of the cross section

$$\frac{dW}{dx} = c_1\alpha\cos(\alpha x) - c_2\alpha\sin(\alpha x) + c_3\beta e^{\beta x} - c_4\beta e^{-\beta x} \quad , \quad (9)$$

and the internal force

$$\begin{cases} M = -(i\omega)^2(e_0a)^2\rho A[c_1\sin(\alpha x) + c_2\cos(\alpha x) + c_3e^{\beta x} \\ +c_4e^{-\beta x}]e^{i\omega t} - [(EI)^* + (e_0a)^2(N+H^0)][-c_1\alpha^2\sin(\alpha x) \\ -c_2\alpha^2\cos(\alpha x) + c_3\beta^2e^{\beta x} + c_4\beta^2e^{-\beta x}]e^{i\omega t} \\ Q = \frac{\partial M}{\partial x} \end{cases} . \quad (10)$$

Simply supported boundary condition at the two ends can be expressed as

$$\begin{cases} w(0,t) = 0, M(0,t) = 0 \\ w(L,t) = 0, M(L,t) = 0 \end{cases} . \quad (11)$$

Substituting Eq. (11) into Eq. (10), we can obtain

$$\begin{cases} c_2 + c_3 + c_4 = 0 \\ -c_2\alpha^2 + c_3\beta^2 + c_4\beta^2 = 0 \\ c_1\sin(\alpha L) + c_2\cos(\alpha L) + c_3e^{\beta L} + c_4e^{-\beta L} = 0 \\ -c_1\alpha^2\sin(\alpha L) - c_2\alpha^2\cos(\alpha L) + c_3\beta^2e^{\beta L} + c_4\beta^2e^{-\beta L} = 0 \end{cases} . \quad (12)$$

To make sure there are nonzero solutions for c_1, c_2, c_3, and c_4, the value of the corresponding coefficient determinant should equal to zero. Thus, we can get

$$\sin(\alpha L) = 0 \Rightarrow \alpha = \frac{n\pi}{L} \quad . \quad (13)$$

Then, Eq. (13) is substituted into Eq. (8) and the circular frequency of nanobeam structure with the simply supported boundary conditions at both ends can be obtained.

As for simply supported boundary conditions at both ends, the deflection of CNTs embedded in the elastic substrate can be further set as

$$w(x,t) = W_{max}\sin(\lambda x)e^{i\omega t} \quad , \quad (14)$$

where $\lambda = n\pi/L$. ω and W_{max} are the circular frequency and the deflection amplitude, respectively. Thus, the corresponding governing equation is

$$\begin{aligned}(EI)^*\frac{\partial^4 w}{\partial x^4} &+ \left[-(N+H^0+k_G)\frac{\partial^2 w}{\partial x^2} + (e_0a)^2(N+H^0+k_G)\frac{\partial^4 w}{\partial x^4}\right] \\ &+ \left[k_W w - (e_0a)^2k_W\frac{\partial^2 w}{\partial x^2}\right] + \left[\rho A\frac{\partial^2 w}{\partial x^2} - (e_0a)^2\rho A\frac{\partial^4 w}{\partial t^2\partial x^2}\right] \\ &+ \left[-\rho I\frac{\partial^4 w}{\partial t^2\partial x^2} + (e_0a)^2\rho I\frac{\partial^6 w}{\partial t^2\partial x^4}\right] = 0 \quad , \end{aligned} \quad (15)$$

where k_W and k_G are the normal Winkler modulus and the Pasternak shear modulus, respectively. Because of thermomechanical coupling effect, the corresponding axial load N consists of two parts: one part (N_M) caused by the axial mechanical preloading and the other part (N_T) caused by thermal expansion or contraction [33]. Hence, the axial load can be given as

$$N = N_M + N_T = N_M - \frac{EA}{1-2\nu}\alpha_x\Delta T \quad , \quad (16)$$

where α_x, ΔT, and ν are the thermal expansion coefficient along the axial direction, the temperature change, and the Poisson ratio, respectively. Substituting Eq. (14) into Eq. (15), we can get

$$\begin{aligned}(EI)^*\lambda^4 &+ (N+H^0+k_G)\lambda^2\left[1+(e_0a)^2\lambda^2\right] \\ &+ k_W\left[1+(e_0a)^2\lambda^2\right] = \rho A\omega^2\left[1+(e_0a)^2\lambda^2\right] \\ &+ \rho I\lambda^2\omega^2\left[1+(e_0a)^2\lambda^2\right] \quad , \end{aligned} \quad (17)$$

and the circular frequency can be given as

$$\omega = \sqrt{\frac{(EI)^*\lambda^4 + (N+H^0+k_G)\lambda^2\left[1+(e_0a)^2\lambda^2\right] + k_W\left[1+(e_0a)^2\lambda^2\right]}{(\rho A + \rho I\lambda^2)\left[1+(e_0a)^2\lambda^2\right]}} . \quad (18)$$

For Euler–Bernoulli beams, the influence of cross-sectional rotary inertia is often ignored. Then, we can get

$$\omega_{EB} = \sqrt{\frac{(EI)^*\lambda^4 + (N+H^0+k_G)\lambda^2\left[1+(e_0a)^2\lambda^2\right] + k_W\left[1+(e_0a)^2\lambda^2\right]}{\rho A\left[1+(e_0a)^2\lambda^2\right]}} . \quad (19)$$

Furthermore, by neglecting surface effect and the influence of elastic substrate, axial preloading and temperature change, the circular frequency is reduced to

https://doi.org/10.1557/jmr.2018.431 Published online by Cambridge University Press

© Materials Research Society 2019

$$\omega_{\mathrm{EB-NL}} = \lambda^2 \sqrt{\frac{EI}{\rho A\left[1+(e_0a)^2\lambda^2\right]}} = \frac{\omega_{\mathrm{EB}}^0}{\sqrt{1+(e_0a)^2\lambda^2}} \quad , \tag{20}$$

which is consistent with the solution from the nonlocal elasticity framework. Herein, $\omega_{\mathrm{EB}}^0 = \lambda^2\sqrt{\frac{EI}{\rho A}}$ is the circular frequency for the classic Euler–Bernoulli beam model.

Modified Timoshenko beam model

For Timoshenko beam, shear deformation and rotary inertia are considered. Similar to the deduction of the modified Euler–Bernoulli beam model, the basic governing equation for the modified Timoshenko beam model is written as

$$\begin{cases} (EI)^* \frac{\partial^2\psi}{\partial x^2} - \kappa GA\left(\frac{\partial w}{\partial x}+\psi\right) = \rho I \frac{\partial^2\psi}{\partial t^2} - (e_0a)^2 \rho I \frac{\partial^4\psi}{\partial t^2\partial x^2} \\ \kappa GA \frac{\partial}{\partial x}\left(\frac{\partial w}{\partial x}+\psi\right) + \left[\left(N+H^0\right)\frac{\partial^2 w}{\partial x^2} - (e_0a)^2(N+H^0)\frac{\partial^4 w}{\partial x^4}\right] \\ +\left[-k_{\mathrm{W}}w + (e_0a)^2 k_{\mathrm{W}}\frac{\partial^2 w}{\partial x^2}\right] + \left[k_{\mathrm{G}}\frac{\partial^2 w}{\partial x^2} - (e_0a)^2 k_{\mathrm{G}}\frac{\partial^4 w}{\partial x^4}\right] \\ = \rho A \frac{\partial^2 w}{\partial t^2} - (e_0a)^2 \rho A \frac{\partial^4 w}{\partial t^2\partial x^2} \quad . \end{cases} \tag{21}$$

As mentioned above, the axial load N is divided into N_{M} and N_{T}. Considering the simple boundary conditions at both ends of CNTs, we can take the deflection expression as

$$w(x,t) = W_{\max}\sin(\lambda x)e^{\mathrm{i}\omega t} \quad , \tag{22}$$

and

$$\psi(x,t) = \Psi_{\max}\cos(\lambda x)e^{\mathrm{i}\omega t} \quad . \tag{23}$$

Herein, $\lambda = n\pi/L$ and ω is the circular frequency. $W_{\max}$ and $\Psi_{\max}$ are the amplitudes of the deflection and the moment slope, respectively. Substituting Eqs. (22) and (23) into Eq. (21), we can obtain

$$\begin{cases} \kappa GA\lambda W_{\max} + \left[(EI)^*\lambda^2 + \kappa GA - \rho I\omega^2 - (e_0a)^2\rho I\lambda^2\omega^2\right] \\ \Psi_{\max} = 0 \\ \left[\begin{array}{l} \kappa GA\lambda^2 + (N+H^0+k_{\mathrm{G}})\lambda^2 + (e_0a)^2(N+H^0+k_{\mathrm{G}})\lambda^4 \\ +k_{\mathrm{W}} + (e_0a)^2 k_{\mathrm{W}}\lambda^2 - \rho A\omega^2 - (e_0a)^2\rho A\lambda^2\omega^2 \end{array}\right] \\ W_{\max} + \kappa GA\lambda\Psi_{\max} = 0 \end{cases} . \tag{24}$$

To make sure that Eq. (24) has nonzero solutions for $W_{\max}$ and $\psi_{\max}$, the coefficient determinant should be zero. In this way, Eq. (24) can be simplified into

$$\begin{aligned} \left(\omega^2\right)^2 &- \frac{(N+H^0+k_{\mathrm{G}})\lambda^2}{\rho A}\omega^2 - \frac{(EI)^*\lambda^2 + \kappa GI\lambda^2 + \kappa GA}{\rho I\left[1+(e_0a)^2\lambda^2\right]}\omega^2 \\ &- \frac{k_{\mathrm{W}}}{\rho A}\omega^2 + \left(N+H^0+k_{\mathrm{G}}\right)\lambda^2\frac{(EI)^*\lambda^2 + \kappa GA}{\rho^2 AI\left[1+(e_0a)^2\lambda^2\right]} \\ &+ \frac{(EI)^*\kappa G\lambda^4}{\rho^2 I\left[1+(e_0a)^2\lambda^2\right]^2} + k_{\mathrm{W}}\frac{(EI)^*\lambda^2 + \kappa GA}{\rho^2 AI\left[1+(e_0a)^2\lambda^2\right]} = 0 \quad . \end{aligned} \tag{25}$$

By solving Eq. (25), we can obtain two circular frequencies (ω_{T1} and ω_{T2}). For the lower circular frequency, the corresponding vibration is flexural vibration; for the higher circular frequency, the corresponding vibration is shear vibration. When the effect of the elastic substrate is neglected, Eq. (25) is converted into

$$\begin{aligned} &\left(\omega^2\right)^2 - \frac{\left(N+H^0\right)\lambda^2}{\rho A}\omega^2 - \frac{(EI)^*\lambda^2+\kappa GI\lambda^2+\kappa GA}{\rho I\left[1+(e_0a)^2\lambda^2\right]}\omega^2 \\ &+(N+H^0)\lambda^2\frac{(EI)^*\lambda^2+\kappa GA}{\rho^2 AI\left[1+(e_0a)^2\lambda^2\right]} + \frac{(EI)^*\kappa G\lambda^4}{\rho^2 I\left[1+(e_0a)^2\lambda^2\right]^2} = 0 \end{aligned} \quad . \tag{26}$$

When the axial load and the surface effect are further ignored, we can obtain the following equation to solve the circular frequency of Timoshenko beam in the nonlocal elasticity framework:

$$\begin{aligned} \frac{E\kappa G}{\rho^2}\lambda^4 - \left[1+(e_0a)^2\lambda^2\right]\left\{\left[\frac{\kappa GA}{\rho I} + \left(\frac{E}{\rho}+\frac{\kappa G}{\rho}\right)\lambda^2\right]\right. \\ \left. -\left[1+(e_0a)^2\lambda^2\right]\omega^2\right\}\omega^2 = 0 \end{aligned} \quad . \tag{27}$$

When $c_1 = \sqrt{E/\rho}$, $c_2 = \sqrt{\kappa G/\rho}$, and $r_0 = \sqrt{I/A}$ are taken, Eq. (27) can be converted into

$$\begin{aligned} c_1^2 r_0^2\lambda^4 - \left[1+(e_0a)^2\lambda^2\right]\left\{1 + r_0^2\left(1+\frac{c_1^2}{c_2^2}\right)\lambda^2\right. \\ \left. -\left[1+(e_0a)^2\lambda^2\right]\frac{r_0^2}{c_2^2}\omega^2\right\}\omega^2 = 0 \end{aligned} \quad . \tag{28}$$

The solution of Eq. (28) is

$$\omega_{\mathrm{T-NL}} = \frac{\omega_{\mathrm{T}}^0}{\sqrt{1+(e_0a)^2\lambda^2}} \quad , \tag{29}$$

where ω_{T}^0 denotes the circular frequency for the classical Timoshenko beam model and can be shown as

$$\omega_{\mathrm{T}}^0 = \sqrt{\frac{1}{2}\left[(c_1^2+c_2^2)\lambda^2 + \frac{c_2^2}{r_0^2}\right] \pm \sqrt{\frac{1}{4}\left[(c_1^2+c_2^2)\lambda^2 + \frac{c_2^2}{r_0^2}\right]^2 - c_1^2c_2^2\lambda^4}} \quad . \tag{30}$$

https://doi.org/10.1557/jmr.2018.431 Published online by Cambridge University Press

© Materials Research Society 2019

Arash et al. [34] pointed out that the influence of the nonlocal small-scale effect on the circular frequency is negligible for the shear force term of Timoshenko beam model. Hence, it can be removed in the following deduction. Based on this point, Eq. (21) can be converted into a more simplified form:

$$\begin{cases} (EI)^* \frac{\partial^2 \psi}{\partial x^2} - \kappa GA\left(\frac{\partial w}{\partial x} + \psi\right) = \rho I\left[\frac{\partial^2 \psi}{\partial t^2} - (e_0 a)^2 \frac{\partial^4 \psi}{\partial t^2 \partial x^2}\right] \\ \kappa GA \frac{\partial}{\partial x}\left(\frac{\partial w}{\partial x} + \psi\right) + (N + H^0)\frac{\partial^2 w}{\partial x^2} = \rho A \frac{\partial^2 w}{\partial t^2} \end{cases} . \tag{31}$$

Additionally, the expressions of internal forces (the bending moment and the shear force) can be reduced to

$$\begin{cases} M = (EI)^* \frac{\partial \psi}{\partial x} - (e_0 a)^2\left[(N + H^0)\frac{\partial^2 w}{\partial x^2} - \rho A \frac{\partial^2 w}{\partial t^2} - \rho I \frac{\partial^3 \psi}{\partial t^2 \partial x}\right] \\ Q = \kappa GA\left(\frac{\partial w}{\partial x} + \psi\right) \end{cases} . \tag{32}$$

The general solution of Eq. (31) can be

$$\begin{cases} w(x,t) = W(x)e^{i\omega t} \\ \psi(x,t) = \Psi(x)e^{i\omega t} \end{cases} . \tag{33}$$

Substituting Eq. (33) into Eq. (31), we can obtain

$$\begin{cases} (EI)^* \frac{\partial^2 \Psi}{\partial x^2} - \kappa GA\left(\frac{\partial W}{\partial x} + \Psi\right) + \omega^2 \rho I\left[\Psi - (e_0 a)^2 \frac{\partial^2 \Psi}{\partial x^2}\right] = 0 \\ \kappa GA\left(\frac{\partial^2 W}{\partial x^2} + \frac{\partial \Psi}{\partial x}\right) + (N + H^0)\frac{\partial^2 W}{\partial x^2} + \omega^2 \rho A W = 0 \end{cases} . \tag{34}$$

By separating variable, we further get

$$\begin{cases} s_1 \frac{d^4 W}{dx^4} + s_2 \frac{d^2 W}{dx^2} + s_3 W = 0 \\ s_1 \frac{d^4 \Psi}{dx^4} + s_2 \frac{d^2 \Psi}{dx^2} + s_3 \Psi = 0 \end{cases} , \tag{35}$$

where $s_1 = \left[(EI)^* - (e_0 a)^2 \omega^2 \rho I\right]\frac{\kappa GA + (N+H^0)}{\kappa GA}$, $s_2 = [(EI)^* - (e_0 a)^2 \omega^2 \rho I]\frac{\omega^2 \rho A}{\kappa GA} + \omega^2 \rho I \frac{\kappa GA + (N+H^0)}{\kappa GA} - (N + H^0)$, and $s_3 = \frac{\omega^2 \rho A}{\kappa GA}(\omega^2 \rho I - \kappa GA)$. The general solution of Eq. (35) can be expressed as

$$\begin{cases} W(x) = c_1 \sin(\alpha x) + c_2 \cos(\alpha x) + c_3 e^{\beta x} + c_4 e^{-\beta x} \\ \Psi(x) = f_1 \sin(\alpha x) + f_2 \cos(\alpha x) + f_3 e^{\beta x} + f_4 e^{-\beta x} \end{cases} . \tag{36}$$

Herein, $\alpha > 0$, $\beta > 0$, $\alpha^2 = \frac{\sqrt{s_2^2 - 4 s_1 s_3} + s_2}{2 s_1}$, and $\beta^2 = \frac{\sqrt{s_2^2 - 4 s_1 s_3} - s_2}{2 s_1} = \frac{\sqrt{s_2^2 - 4 s_1 s_3}}{s_1} - \alpha^2$. Substituting Eq. (36) into Eq. (31), the coefficient relationships can be shown as

$$\begin{cases} f_1 = \Omega_\alpha c_2,\ f_2 = -\Omega_\alpha c_1,\ \Omega_\alpha = \left[\alpha + \alpha \frac{(N+H^0)}{\kappa GA} - \frac{\omega^2 \rho A}{\alpha \kappa GA}\right] \\ f_3 = -\Omega_\beta c_3,\ f_4 = \Omega_\beta c_4,\ \Omega_\beta = \left[\beta + \beta \frac{(N+H^0)}{\kappa GA} + \frac{\omega^2 \rho A}{\beta \kappa GA}\right] \end{cases} . \tag{37}$$

Based on the modified Timoshenko beam model, the vibration analysis of single-walled CNTs is converted to the determination of the unknown coefficients in Eq. (36) with simply supported boundary condition at the two ends. To obtain the circular frequency, we only need to solve the governing equation with the condition that the coefficient determinants equal to zero. For simplification, Eq. (32) can be converted into

For the simply supported boundary conditions at both ends, by combining Eqs. (11) and (38), we can obtain

To make sure there are nonzero solutions for c_i (i = 1–4) and f_j (j = 1–4), the corresponding coefficient determinant should equal to zero. Thus, we can get

$$\sin(\alpha L) = 0 \Rightarrow \alpha = \frac{n\pi}{L} . \tag{40}$$

According to the correlation between α and ω, the circular frequency for the simply supported boundary conditions at both ends is obtained. In this way, the governing equations of the circular frequency can be solved, without considering the influence of nonlocal small-scale effect on the shearing term of Timoshenko beam model.

Numerical results and discussion

For the vibration analysis of single-walled CNT embedded in the elastic substrate, the circular frequency for the modified Euler–Bernoulli beam model is illustrated as Eq. (19), whereas

$$\begin{cases} M = \left[(EI)^* - (e_0 a)^2 \rho I \omega^2\right]\left[f_1 \alpha \cos(\alpha x) - f_2 \alpha \sin(\alpha x) + f_3 \beta e^{\beta x} - f_4 \beta e^{-\beta x}\right] e^{i\omega t} \\ -(e_0 a)^2 (N + H^0)\left[-c_1 \alpha^2 \sin(\alpha x) - c_2 \alpha^2 \cos(\alpha x) + c_3 \beta^2 e^{\beta x} + c_4 \beta^2 e^{-\beta x}\right] e^{i\omega t} \\ -(e_0 a)^2 \rho A \omega^2 \left[c_1 \sin(\alpha x) + c_2 \cos(\alpha x) + c_3 e^{\beta x} + c_4 e^{-\beta x}\right] e^{i\omega t} \\ Q = \kappa GA \begin{bmatrix} c_1 \alpha \cos(\alpha x) - c_2 \alpha \sin(\alpha x) + c_3 \beta e^{\beta x} - c_4 \beta e^{-\beta x} \\ + f_1 \sin(\alpha x) + f_2 \cos(\alpha x) + f_3 e^{\beta x} + f_4 e^{-\beta x} \end{bmatrix} e^{i\omega t} \end{cases} . \tag{38}$$

https://doi.org/10.1557/jmr.2018.431 Published online by Cambridge University Press

© Materials Research Society 2019

$$\begin{cases} c_2 + c_3 + c_4 = 0 \\ \left[(EI)^* - (e_0a)^2\rho I\omega^2\right](f_1\alpha + f_3\beta - f_4\beta) \\ -(e_0a)^2(N + H^0)\left(-c_2\alpha^2 + c_3\beta^2 + c_4\beta^2\right) - (e_0a)^2\rho A\omega^2(c_2 + c_3 + c_4) = 0 \\ c_1\sin(\alpha L) + c_2\cos(\alpha L) + c_3e^{\beta L} + c_4e^{-\beta L} = 0 \\ \left[(EI)^* - (e_0a)^2\rho I\omega^2\right]\left[f_1\alpha\cos(\alpha L) - f_2\alpha\sin(\alpha L) + f_3\beta e^{\beta L} - f_4\beta e^{-\beta L}\right] \\ -(e_0a)^2(N + H^0)\left[-c_1\alpha^2\sin(\alpha L) - c_2\alpha^2\cos(\alpha L) + c_3\beta^2e^{\beta L} + c_4\beta^2e^{-\beta L}\right] \\ -(e_0a)^2\rho A\omega^2\left[c_1\sin(\alpha L) + c_2\cos(\alpha L) + c_3e^{\beta L} + c_4e^{-\beta L}\right] = 0 \end{cases} . \quad (39)$$

that for the modified Timoshenko beam model originates from the positive root of Eq. (25). Herein, the larger positive root corresponds to the circular frequency of the shear vibration, whereas the smaller one is related to the flexural vibration (the research focus in our work). When small-scale effect and surface effect are neglected, the above frequency solutions can be degraded to the circular frequencies for the classical Euler–Bernoulli and Timoshenko beam models, respectively. When the effects of elastic substrate, temperature change, and axial preloading are further removed, we can obtain the circular frequencies of the corresponding Euler–Bernoulli beam and Timoshenko beam under the classical theoretical framework (i.e., ω_{EB}^0 and ω_T^0).

For single-walled CNTs, the representative parameters used in the numerical experiments are selected as follows [35, 36]: bulk Young's modulus $E = 5.5$ TPa, wall thickness $t = 0.066$ nm, nonlocal material parameter $e_0 = 0.39$, internal characteristic length $a = 0.142$ nm, residual surface stress $\tau_0 = 25$ nN/nm, surface modulus $S = 50$ nN/nm, thermal expansion coefficient $\alpha_x = -1.6 \times 10^{-6}$ K^{-1} at room or low temperature, and $\alpha_x = 1.1 \times 10^{-6}$ K^{-1} at high temperature.

Generally, the chiral vector of single-walled CNT is taken as (9,9) and the corresponding diameter (d) is 1.22 nm. In addition, the length–diameter ratio (L/d) is set as 12. Figure S1 in the Supplementary material shows the dependence of circular frequency on the vibration mode order n for different beam models. For both the classical and the modified beam models, the circular frequencies of single-walled CNTs increase with the increase of the vibration mode order. In addition, the computational results for the modified beam models are larger than the corresponding results for the classical beam models. Thus, small-scale effect and surface effect have non-negligible influences on the circular frequency. For the flexural vibration with a low vibration mode order, the circular frequency of Euler–Bernoulli beam is slightly higher than that of Timoshenko beam. As the vibration mode order (n) increases continuously, the circular frequency of Euler–Bernoulli beam model rises rapidly and the difference between these two models are also expanded. Compared with Timoshenko beam model, Euler–Bernoulli beam model is more sensitive to the vibration mode order. To further investigate the influence of the vibration mode order on size effect, we trace the evolution of circular frequency ratios in Fig. S2. Herein, the ratios of circular frequency reflect the size effect to some extent and are defined as

$$\begin{cases} r_{EB} = \frac{\omega_{EB}}{\omega_{EB}^0} \\ r_T = \frac{\omega_T}{\omega_T^0} \end{cases} , \quad (41)$$

where r_{EB} and r_T denote the ratios of frequency for Euler–Bernoulli beam and Timoshenko beam, respectively. ω_{EB}, ω_{EB}^0, ω_T, and ω_T^0 represent the circular frequencies for the modified Euler–Bernoulli beam models, the classical Euler–Bernoulli beam model, the modified Timoshenko beam model, and the classical Timoshenko beam model, respectively. For flexural vibration, size effect is more significant when the vibration mode order is low; for shear vibration, size effect evolves nonlinearly with the increase of the vibration mode order, and there is the most optimized vibration mode order, which corresponds to the most significant size effect.

In addition, we take $n = 2$ to investigate the effects of nonlocal small-scale effect parameter e_0, surface modulus S, and residual surface stress τ_0 on the circular frequency of single-walled CNTs. The results are shown in the Supplementary material (Figs. S3–S5). For flexural vibration, the computational results for the modified Euler–Bernoulli beam model are much larger than those for the modified Timoshenko beam, which is consistent with the case for the classical beam models. According to Fig. S3, with the increase of e_0, the circular frequencies of single-walled CNTs decrease for both flexural vibration and shear vibration. On the contrary, such a trend reverses for the cases of surface modulus S (Fig. S4) and residual surface stress τ_0 (Fig. S5). Among these three factors, the effect of τ_0 is most significant. Compared with surface effect

https://doi.org/10.1557/jmr.2018.431 Published online by Cambridge University Press

© Materials Research Society 2019

(represented by S and τ_0), the small-scale effect (shown in the case of e_0) plays an opposite role in the evolution of circular frequency; namely, small-scale effect makes single-walled CNT "softer" and thus easier to vibrate, whereas surface effect makes it "harder" and more difficult to vibrate. Thus, the flexural vibration of CNTs are influenced by these two effects at the same time. For shear vibration, similar conclusions are obtained, whereas the effect of e_0 is the "strongest," compared with that of S and τ_0.

Effect of structural dimensions

Figures 1–3 illustrate the effects of structural dimensions on the ratio of circular frequency (i.e., size effect) for the modified Euler–Bernoulli and Timoshenko beam models. With CNT's diameter unchanged, the length–diameter ratio increases when CNT's length increases and vice versa. As shown in Fig. 1(a) (flexural vibration), the circular frequency ratio increases with the length increasing, indicating an increasingly significant size effect. On the contrary, the reversed trend is demonstrated in Fig. 1(b) (shear vibration). For the flexural vibration, the rising rate of the circular frequency ratio is faster when the vibration mode order is lower; for the shear vibration, the higher the vibration mode order is, the faster the circular frequency ratio increases. Therefore, when CNT's diameter is constant, its length has a remarkable influence on the size dependence of CNT's vibration analysis.

Similarly, with CNT's length constant (Fig. 2), the circular frequency ratios evolve in the opposite trends for flexural vibration and shear vibration. For flexural vibration [Fig. 2(a)], as CNT's diameter increases, the length–diameter ratio decreases, whereas size effect weakens significantly. For shear vibration [Fig. 2(b)], size effect is strengthened with the increase of CNT's diameter. Therefore, the relationships between the performance of size effect and the length–diameter ratio are similar in both Figs. 1 and 2.

To further investigate the relationship between the circular frequency ratio and the length–diameter ratio, we keep the length–diameter ratio constant and change CNT's diameter and its length at the same time. The results are demonstrated in Fig. 3. For flexural vibration [Fig. 3(a)], size effect becomes more prominent with the decrease of CNT's diameter. Such

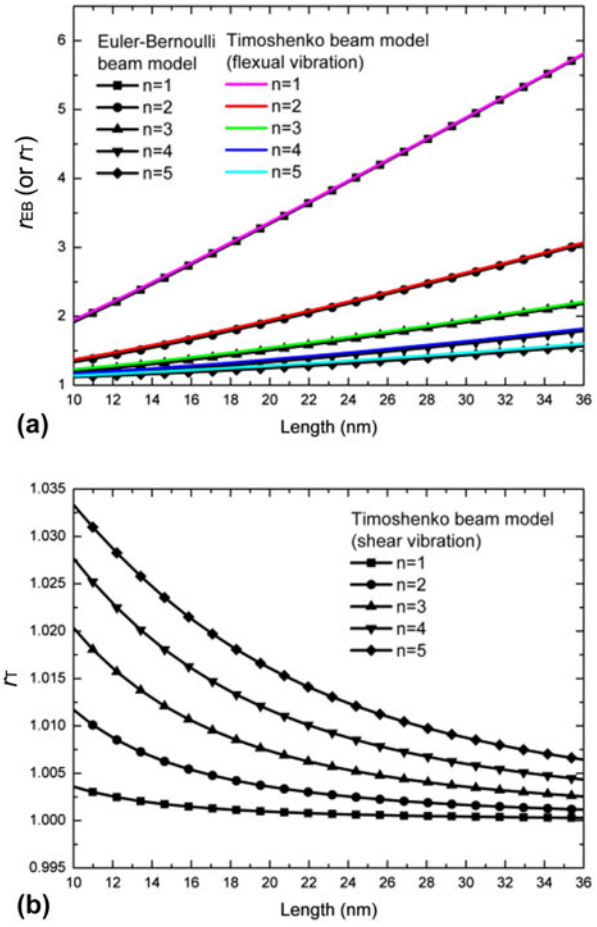


Figure 1: The circular frequency ratio as a function of CNT's length (constant diameter) for (a) flexural vibration and (b) shear vibration.

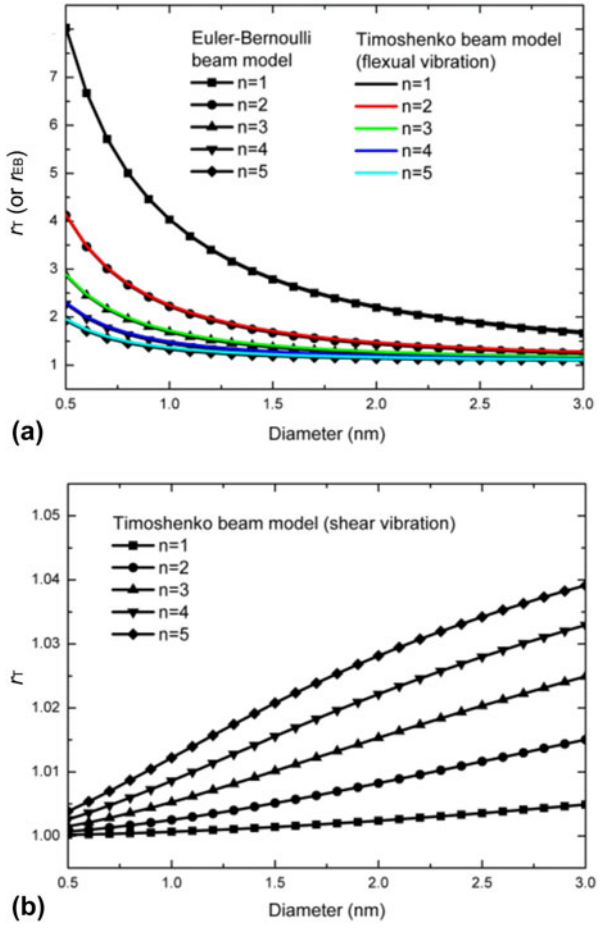


Figure 2: The circular frequency ratio as a function of CNT's diameter (constant length) for (a) flexural vibration and (b) shear vibration.

https://doi.org/10.1557/jmr.2018.431 Published online by Cambridge University Press

© Materials Research Society 2019

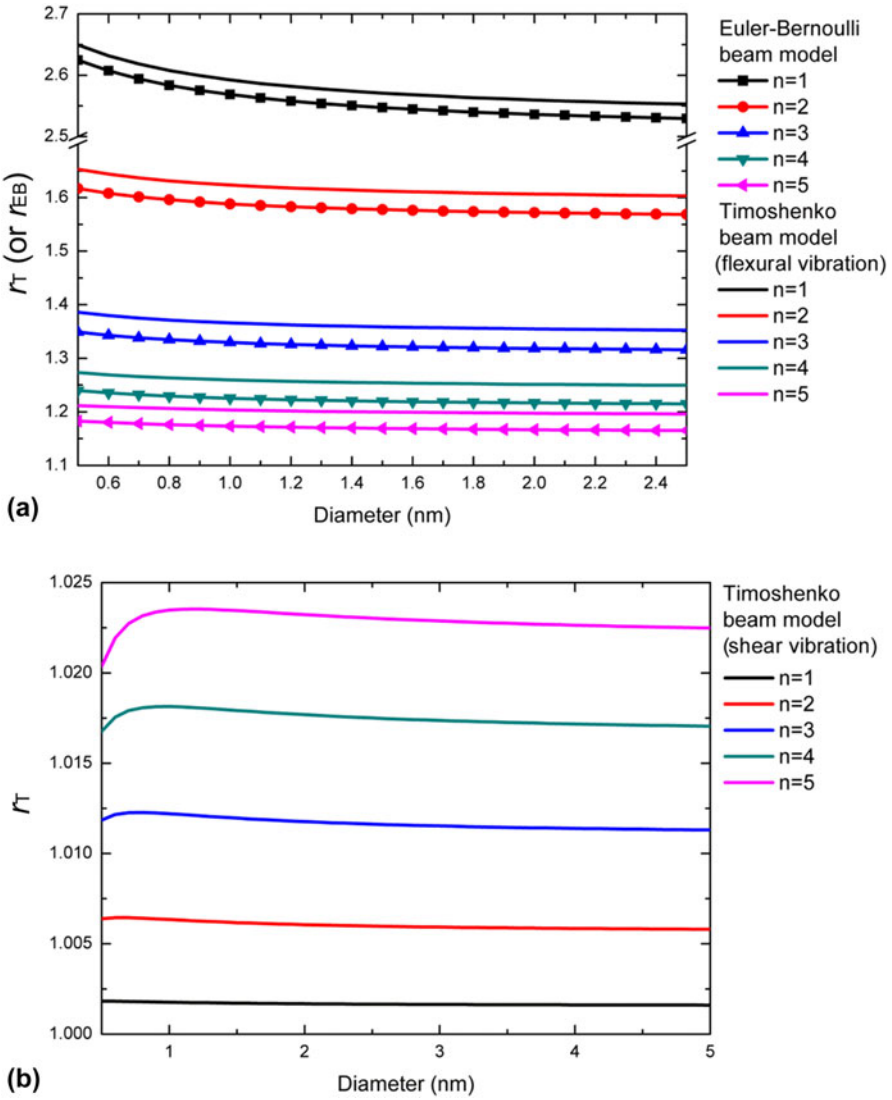


Figure 3: The circular frequency ratio as a function of CNT's diameter (constant length–diameter ratio) for (a) flexural vibration and (b) shear vibration.

a phenomenon is further strengthened when the vibration mode order is low. For shear vibration [Fig. 3(b)], when the vibration mode order is lower (e.g., $n = 1$–2), there is a similar trend for the relationship between CNT's circular frequency ratio and its diameter. However, when the vibration mode order is higher (e.g., $n > 2$), the nonlinear correlation between the circular frequency ratio and CNT's diameter exists. For a given vibration mode order, there is a typical diameter, which corresponds to the "strongest" size effect.

Effect of elastic substrate modulus

In many project cases, CNTs are embedded in the elastic substrates. Thus, it is necessary to investigate the impact of elastic substrate properties on the circular frequency and the ratio of frequency (i.e., the strength of size effect). Herein, we focus on the flexural vibration of CNTs, and two important parameters for elastic substrate (Winkler modulus K_W and Pasternak shear modulus k_G) are considered.

According to Figs. 4 and S6, for a given vibration mode order, the circular frequency of single-walled CNTs increases with the increase of Winkler modulus K_W, suggesting that a larger Winkler modulus suppresses the vibration of single-walled CNTs and enhances their circular frequency. It should be noted that when the vibration mode order is low, the calculation results for Euler–Bernoulli beam model approximate to those of Timoshenko beam model. As the vibration mode order further increases, the frequency difference between these two models is enlarged (Fig. 4).

Figure 5 shows the variation of the circular frequency ratios (r_{EB} or r_T) with respect to Winkler modulus K_W. Obviously, the frequency ratio, proportional to the strength of size effect, gradually decreases with the increase of Winkler modulus K_W.

https://doi.org/10.1557/jmr.2018.431 Published online by Cambridge University Press

© Materials Research Society 2019

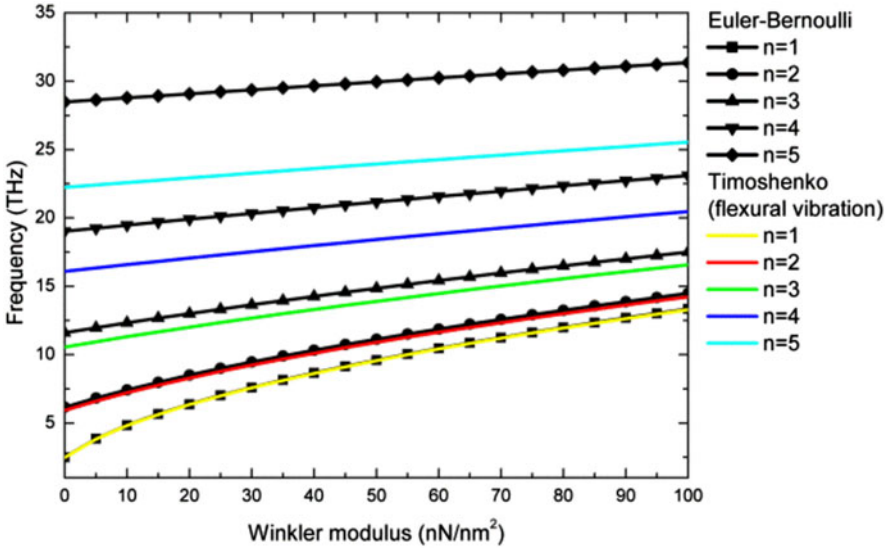


Figure 4: The circular frequency as a function of Winkler modulus for different beam models.

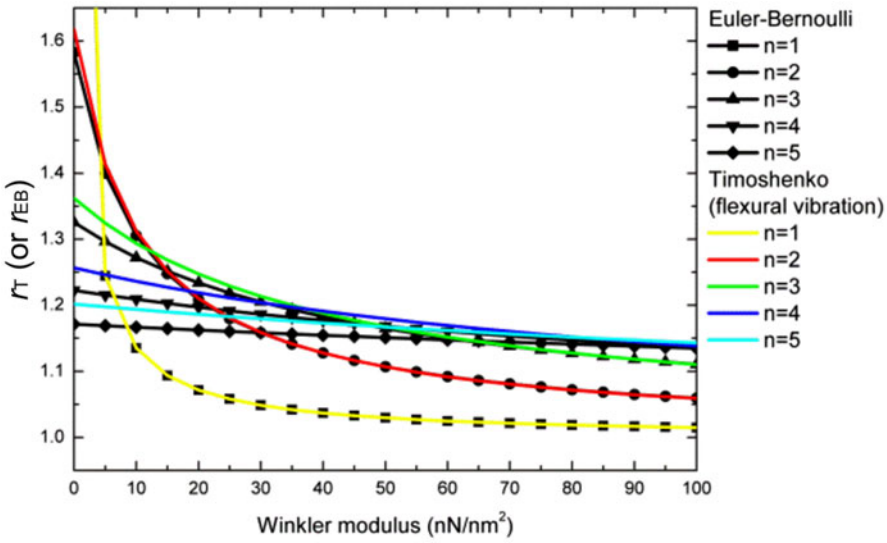


Figure 5: The circular frequency ratio as a function of Winkler modulus for different beam models.

The lower the vibration mode order is, the more rapidly the frequency ratio decreases. Specifically, for n = 1–2, as K_W increases, the ratio of circular frequency drops first at a fast rate and then approaches 1 gradually at a much slower rate. For a larger n, the ratio of frequency decreases gently with the enhancement of K_W. Therefore, when Winkler modulus K_W is small, its slight change has a remarkable influence on the size effect of single-walled CNTs and cannot be ignored. Similar to the results in Fig. 4, the frequency difference between these two models is obvious when vibration mode order is high.

Furthermore, the effects of Pasternak shear modulus k_G on the vibration characteristics of CNTs are demonstrated in Figs. S7–S9. The calculation results are similar to those for Winkler modulus K_W. As shown in Fig. S7–S8, the circular frequency increases with the increase of Pasternak shear modulus k_G. The lower the vibration mode order is, the smaller the frequency difference between Euler–Bernoulli beam model and Timoshenko beam model is. In Fig. S9, the ratio of frequency decreases with the increase of Pasternak shear modulus k_G. Similar to Winkler modulus K_W, when Pasternak shear modulus k_G is low, its slight change influences the frequency ratio (i.e., size effect) significantly. Additionally, as Pasternak shear modulus k_G increases, the ratio of circular frequency approaches 1.

Effect of temperature change

Temperature change is the most common environmental factor for the applications of many nanodevices involving CNTs, and

https://doi.org/10.1557/jmr.2018.431 Published online by Cambridge University Press

© Materials Research Society 2019

its influence on the mechanical behavior of CNTs has been analyzed by many researchers [33, 37]. Generally, we investigate the vibration response of CNTs at high temperature and the effects of temperature change on the circular frequency and the frequency ratio. In addition, the thermal expansion coefficient of CNTs is positive at high temperature, but negative at room or low temperature. Therefore, we can deduce an opposite conclusion for the cases at room or low temperature, according to the results at high temperature. Herein, only flexural vibration is discussed.

Based on the elastic substrate correlation term in the modified Euler–Bernoulli and Timoshenko beam models, we can conclude that the circular frequency of single-walled CNTs decreases with the increase of temperature changes. An example with $n = 2$ is shown in Fig. S10. The effect of temperature change on the frequency ratio is demonstrated in Fig. 6, where the frequency ratio rises with the temperature change increasing. For a given vibration mode order, the curves for the frequency ratio of the Timoshenko beam model always lie above those for the Euler–Bernoulli beam model. When the vibration mode order is lower, the corresponding frequency ratio varies greatly for the same temperature range. Therefore, when the value of temperature change is positive and large, it plays an important role in the performance of size effect.

Effect of axial preloading

The practical serving environment of CNTs is sophisticated. In many cases, axial preloadings can be caused by temperature change or assembly error. Therefore, it is of great importance to investigate the influence of different preloadings on the vibration behavior of CNTs. Herein, we discuss the effects of axial preloadings on the flexural circular frequency and the frequency ratio of single-walled CNTs. Based on the modified beam models we derive, the effect of axial preloading is consistent with that of Pasternak shear modulus k_G. The only difference is that the value of preload can be positive (pretensile loading) or negative (precompressive loading), whereas Pasternak shear modulus can only take a positive value.

Figure 7 depicts the dependence of the circular frequency on the vibration mode order for different beam models with various preloads. According to Fig. 7, the axial pretensile loading enhances the circular frequency of single-walled CNTs, whereas the axial precompressive loading reduces the corresponding frequency. For a much larger precompressive loading, the positive root for the solution of circular frequency may not exist, because such a stress level restrains CNT's flexural vibration severely and makes its buckling destruction easier to take place. More details are shown in Fig. S11. For a given vibration mode order, the circular frequency increases with the increase of the preload, and the frequency corresponding to modified Euler–Bernoulli beam model is higher than that for the Timoshenko beam model. The difference is enlarged, as the vibration mode order increases. Additionally, the circular ratio as a function of axial preloadings is also illustrated in Fig. 8. It is easy to find that the effect of the axial precompressive loading on the circular frequency ratio is much more significant than that of the axial pretensile loadings. As the axial precompressive loading increases, the circular frequency ratio rises sharply, and a larger precompressive loading may lead to the termination of vibration and the initiation of buckling behavior, which corresponds to no

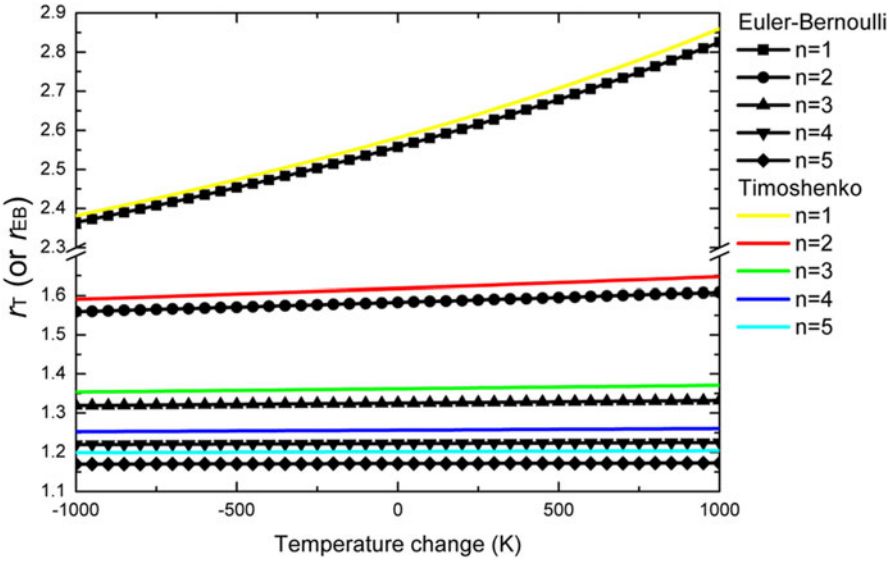


Figure 6: The circular frequency ratio as a function of temperature change for different beam models.

https://doi.org/10.1557/jmr.2018.431 Published online by Cambridge University Press

© Materials Research Society 2019

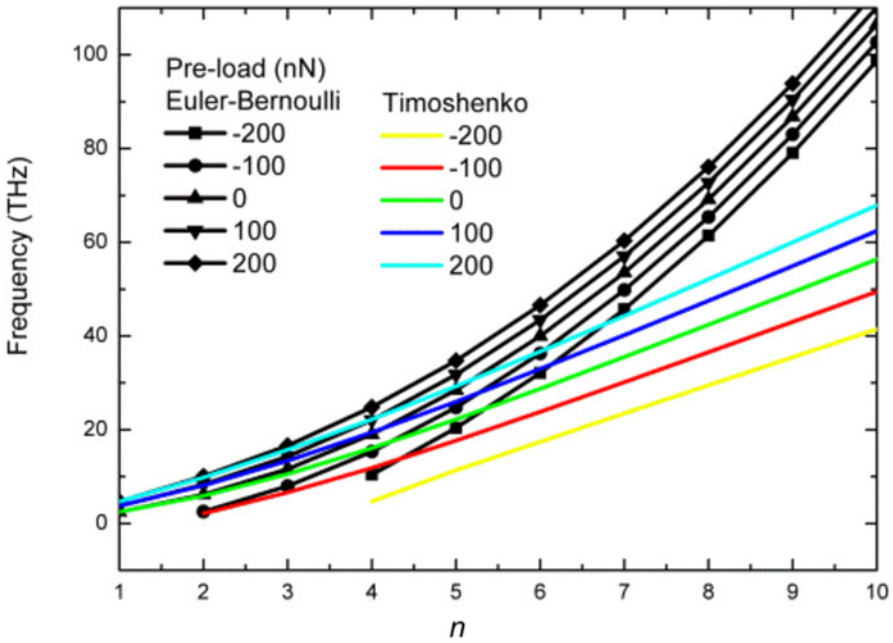


Figure 7: The circular frequency as a function of vibration mode order for different beam models with various preloads.

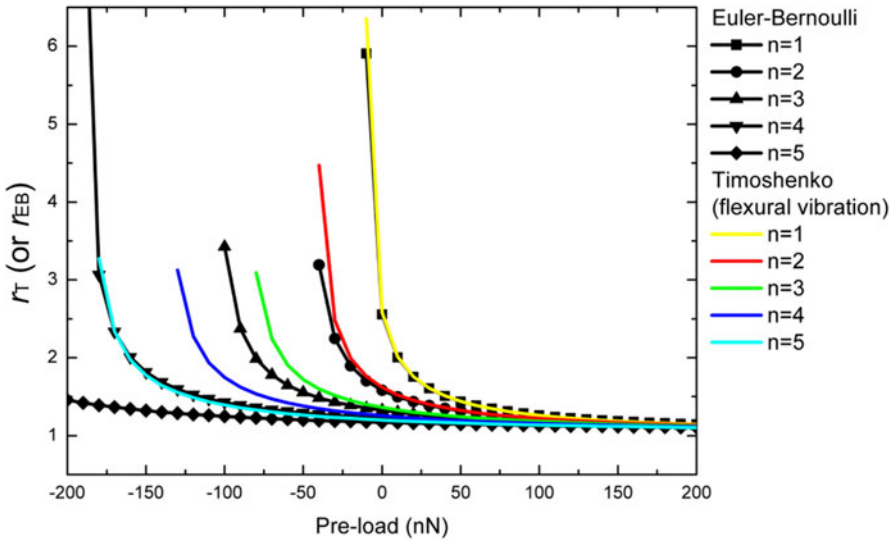


Figure 8: The circular frequency ratio as a function of preload for different beam models.

real solution for the circular frequency. On the contrary, with the increase of the axial pretensile loading, the ratio of circular frequency drops gradually, i.e., size effect gradually weakens.

Conclusions

By deriving the modified Euler–Bernoulli and Timoshenko beam models for CNT's vibration behaviors and carrying out the numerical experiments, we have investigated symmetrically the influences of nonlocal small-scale effect and surface effect on the vibration response of CNTs. Our main conclusions are

(1) The size effect is directly related to the structure dimensions of CNTs. For flexural vibration, size effect, represented by the circular frequency ratio of single-walled CNT, decreases with the increase of its diameter, but increases with the increase of the length–diameter ratio; for shear vibration with n = 1–2, size effect weakens, as CNT's diameter and length–diameter ratio increase.

https://doi.org/10.1557/jmr.2018.431 Published online by Cambridge University Press

© Materials Research Society 2019

(2) For flexural vibration, the circular frequency is positively correlated with Winkler modulus and Pasternak shear modulus, indicating that the elastic substrate restrains CNT's vibration to some extent. In addition, size effect is strengthened with the decreases of Winkler modulus and Pasternak shear modulus.

(3) For flexural vibration at high temperature, the circular frequency of single-walled CNT decreases with the increase of temperature change, suggesting that temperature rise promotes the vibration response. On the other hand, the ratio of the circular frequency (i.e., the intensity of size effect) is enhanced with the increase of temperature change, suggesting that temperature rise strengthens size effect. According to the thermal expansion characteristics of CNTs, the corresponding results for room or low temperature are opposite to those for high temperature.

(4) The axial preloading has an important influence on the flexural circular frequency and the performance of size effect. The precompressive loading reduces the flexural circular frequency, but promotes the performance of size effect; the pretensile loading enhances the flexural circular frequency, but has little impact on the size dependence of CNT's vibration response.

(5) The lower the vibration mode order is, the closer the results from the modified Euler–Bernoulli and Timoshenko beam models are. Meanwhile, the effects of different factors, including elastic substrate, temperature change, and axial preloading, are more significant at a low vibration mode order.

Acknowledgments

This work was partially supported by the National Natural Science Foundation of China (Nos. 11672110, 11472110, and 11372113), the Natural Science Foundation of Guangdong Province (No. 2017A030313014), and the open projects of State Key Laboratory for Strength and Vibration of Mechanical Structures (Xi'an Jiaotong University) (No. SV2017-KF-04).

Supplementary material

To view supplementary material for this article, please visit https://doi.org/10.1557/jmr.2018.431.

References

1. **F. Li, H.M. Cheng, S. Bai, G. Su, and M.S. Dresselhaus**: Tensile strength of single-walled carbon nanotubes directly measured from their macroscopic ropes. *Appl. Phys. Lett.* **77**, 3161–3163 (2000).
2. **K. Liu, Y. Sun, R. Zhou, H. Zhu, J. Wang, L. Liu, S. Fan, and K. Jiang**: Carbon nanotube yarns with high tensile strength made by a twisting and shrinking method. *Nanotechnology* **21**, 045708 (2010).
3. **X. Zhang, Q. Li, T.G. Holesinger, P.N. Arendt, J. Huang, P.D. Kirven, T.G. Clapp, R.F. Depaula, X. Liao, and Y. Zhao**: Ultrastrong, stiff, and lightweight carbon-nanotube fibers. *Adv. Mater.* **19**, 4198–4201 (2010).
4. **M.M.J. Treacy, T.W. Ebbesen, and J.M. Gibson**: Exceptionally high Young's modulus observed for individual carbon nanotubes. *Nature* **381**, 678–680 (1996).
5. **A. Jorio, G. Dresselhaus, and M.S. Dresselhaus**: Carbon nanotubes: Advanced topics in the synthesis, structure, properties and applications. *Mater. Today* **11**, 52–60 (2008).
6. **C. Li and T.W. Chou**: Single-walled carbon nanotubes as ultrahigh frequency nanomechanical resonators. *Phys. Rev. B* **68**, 338–344 (2003).
7. **C. Li and T.W. Chou**: Mass detection using carbon nanotube-based nanomechanical resonators. *Appl. Phys. Lett.* **84**, 5246–5248 (2004).
8. **A. Lohrasebi and H. Rafii-Tabar**: Computational modeling of an ion-driven nanomotor. *J. Mol. Graphics Modell.* **27**, 116–123 (2008).
9. **J. Han, A. Globus, R. Jaffe, and G. Deardorff**: Molecular dynamics simulations of carbon nanotube-based gears. *Nanotechnology* **8**, 95–102 (1997).
10. **A.M. Fennimore, T.D. Yuzvinsky, W.Q. Han, M.S. Fuhrer, J. Cumings, and A. Zettl**: Rotational actuators based on carbon nanotubes. *Nature* **424**, 408 (2003).
11. **S.S. Durov and O.V. Ogloblya**: Molecular dynamics simulation of mechanical, vibrational and electronic properties of carbon nanotubes. *Comput. Mater. Sci.* **17**, 352–355 (2000).
12. **W.H. Duan, C.M. Wang, and Y.Y. Zhang**: Calibration of nonlocal scaling effect parameter for free vibration of carbon nanotubes by molecular dynamics. *J. Appl. Phys.* **101**, 195412–196312 (2007).
13. **L. Wang, H. Hu, and W. Guo**: Thermal vibration of carbon nanotubes predicted by beam models and molecular dynamics. *Proc. R. Soc. London, Ser. A* **466**, 2325–2340 (2010).
14. **R. Ansari, S. Ajori, and B. Arash**: Vibrations of single- and double-walled carbon nanotubes with layerwise boundary conditions: A molecular dynamics study. *Curr. Appl. Phys.* **12**, 707–711 (2012).
15. **I. Chang**: Molecular dynamics investigation of carbon nanotube resonance. *Modell. Simul. Mater. Sci. Eng.* **21**, 045011 (2013).
16. **R. Liu and L. Wang**: Thermal vibration of a single-walled carbon nanotube predicted by semiquantum molecular dynamics. *Phys. Chem. Chem. Phys.* **17**, 5194–5201 (2015).
17. **Y.Q. Zhang, G.R. Liu, and X.Y. Xie**: Free transverse vibrations of double-walled carbon nanotubes using a theory of nonlocal elasticity. *Phys. Rev. B* **71**, 195404 (2005).
18. **Q. Wang and V.K. Varadan**: Vibration of carbon nanotubes studied using nonlocal continuum mechanics. *Smart Mater. Struct.* **15**, 659 (2006).

https://doi.org/10.1557/jmr.2018.431 Published online by Cambridge University Press

© Materials Research Society 2019

19. **C.M. Wang, V.B.C. Tan, and Y.Y. Zhang**: Timoshenko beam model for vibration analysis of multi-walled carbon nanotubes. *J. Sound Vib.* **294**, 1060–1072 (2006).
20. **P. Lu, H.P. Lee, C. Lu, and P.Q. Zhang**: Application of nonlocal beam models for carbon nanotubes. *Int. J. Solid Struct.* **44**, 5289–5300 (2007).
21. **R. Ansari and S. Sahmani**: Small scale effect on vibrational response of single-walled carbon nanotubes with different boundary conditions based on nonlocal beam models. *Commun. Nonlinear Sci. Numer. Simulat.* **17**, 1965–1979 (2012).
22. **J. Yoon, C.Q. Ru, and A. Mioduchowski**: Vibration of an embedded multiwall carbon nanotube. *Compos. Sci. Technol.* **63**, 1533–1542 (2003).
23. **S.C. Pradhan and T. Murmu**: Small-scale effect on vibration analysis of single-walled carbon nanotubes embedded in an elastic medium using nonlocal elasticity theory. *J. Appl. Phys.* **105**, 56 (2009).
24. **K.B. Mustapha and Z.W. Zhong**: Free transverse vibration of an axially loaded non-prismatic single-walled carbon nanotube embedded in a two-parameter elastic medium. *Comput. Mater. Sci.* **50**, 742–751 (2011).
25. **A. Benzair, A. Tounsi, A. Besseghier, H. Heireche, N. Moulay, and L. Boumia**: The thermal effect on vibration of single-walled carbon nanotubes using nonlocal Timoshenko beam theory. *J. Phys. D: Appl. Phys.* **41**, 225404 (2008).
26. **Y. Zhang, G. Liu, and H. Xu**: Transverse vibrations of double-walled carbon nanotubes under compressive axial load. *Phys. Lett. A* **340**, 258–266 (2005).
27. **T. Murmu and S. Adhikari**: Scale-dependent vibration analysis of prestressed carbon nanotubes undergoing rotation. *J. Appl. Phys.* **108**, 250 (2010).
28. **J. Tersoff**: Modeling solid-state chemistry: Interatomic potentials for multicomponent systems. *Phys. Rev. B* **39**, 5566–5568 (1989).
29. **D.W. Brenner, O.A. Shenderova, J.A. Harrison, S.J. Stuart, B. Ni, and S.B. Sinnott**: A second-generation reactive empirical bond order (REBO) potential energy expression for hydrocarbons. *J. Phys.: Condens. Matter* **14**, 783 (2002).
30. **S.J. Stuart, A.B. Tutein, and J.A. Harrison**: A reactive potential for hydrocarbons with intermolecular interactions. *J. Chem. Phys.* **112**, 6472–6486 (2000).
31. **A.C. Eringen**: On differential equations of nonlocal elasticity and solutions of screw dislocation and surface waves. *J. Appl. Phys.* **54**, 4703–4710 (1998).
32. **X.Q. Zhang, X.H. Yao, and Y.G. Sun**: Scale effect on flexural wave propagation in embedded single-walled carbon nanotubes: Nonlocal small-size effect and surface effect. *J. Comput. Theor. Nanosci.* **12**, 2356–2365 (2015).
33. **Y.Q. Zhang, X. Liu, and J.H. Zhao**: Influence of temperature change on column buckling of multiwalled carbon nanotubes. *Phys. Lett. A* **372**, 1676–1681 (2008).
34. **B. Arash and Q. Wang**: A review on the application of nonlocal elastic models in modeling of carbon nanotubes and graphenes. *Comput. Mater. Sci.* **51**, 303–313 (2012).
35. **Y.G. Sun, X.H. Yao, Y.J. Liang, and Q. Han**: Nonlocal beam model for axial buckling of carbon nanotubes with surface effect. *Europhys. Lett.* **99**, 56007 (2012).
36. **X.H. Yao and Y.G. Sun**: Combined bending stability of carbon nanotubes subjected to thermo-electro-mechanical loadings. *Comput. Mater. Sci.* **54**, 135–144 (2012).
37. **X.H. Yao and Q. Han**: Investigation of axially compressed buckling of a multi-walled carbon nanotube under temperature field. *Compos. Sci. Technol.* **67**, 125–134 (2007).

https://doi.org/10.1557/jmr.2018.431 Published online by Cambridge University Press

© Materials Research Society 2019